T-type Inverter in both Continuous and Discontinuous Current Mode for Active Power Decoupling Capability

Ryohei Higashide
Dept. of Electrical, Electronics, and Information Engineering
Nagaoka University of Technology
Nagaoka, Japan
s235027@stn.nagaokaut.ac.jp

Rintaro Kusui
Dept. of Electrical, Electronics, and Information Engineering
Nagaoka University of Technology
Nagaoka, Japan
kusui@stn.nagaokaut.ac.jp

Hiroki Watanabe
Dept. of Electrical, Electronics, and Information Engineering
Nagaoka University of Technology
Nagaoka, Japan
hwatanabe@vos.nagaokaut.ac.jp

Yuki Nakata
Dept. of Electrical, Electronics, and Information Engineering
Nagaoka University of Technology
Nagaoka, Japan
ynakata@vos.nagaokaut.ac.jp

Jun-ichi Itoh
Dept. of Electrical, Electronics, and Information Engineering
Nagaoka University of Technology
Nagaoka, Japan
itoh@vos.nagaokaut.ac.jp

***Abstract*— This paper proposes an active power decoupling (APD) method with both continuous and discontinuous current modes for a T-type inverter, which does not require additional components. The operation in continuous current mode (CCM) has uncontrollable periods of neutral point current for APD. On the other hand, the operation in discontinuous current mode (DCM) decreases efficiency due to an increase in the RMS value of the inductor current. The proposed method switches from CCM to DCM in the uncontrollable periods of the neutral current to reduce the inductor current RMS. However, the efficiency improvement effect is limited because the losses are too large in the DCM period. Therefore, the efficiency improvement method is applied to the CCM/DCM operation. The experimental result indicates that the efficiency improvement method improves the efficiency from 90.1% to 92.5%. In addition, the proposed CCM/DCM control reduces the second harmonic components of the input current by 90.1% compared with not using the APD operation.**

Keywords—T-type inverter, Continuous current mode, Discontinuous current mode, Active power decoupling

I. INTRODUCTION

Photovoltaic (PV) systems have recently been actively researched as a sustainable power solution. PV systems need power conditioning systems (PCS) to utilize PV-generated power [1]. Typically, the PCS consists of the DC/DC converter and the inverter in order to connect the PV panels to the single-phase AC grid. PV systems require PCS to have a low cost, a long lifetime, and a small volume.

Power pulsation occurs on the DC side at twice the grid frequency in a single-phase inverter. Power pulsation decreases the performance of the maximum power point tracking (MPPT). Hence, the bulky electrolytic capacitor is usually used in the DC link to absorb the power pulsation. However, electrolytic capacitors limit the lifetime of the power converter according to the Arrhenius law [2].

The active power decoupling (APD) compensates for the power pulsation with small buffer capacitors by the large fluctuation of capacitor voltage. As a result, APD replaces the electrolytic capacitance with small capacitors with no lifetime, such as film or ceramic capacitors [3]-[9]. Consequently, APD methods reduce the volume and extend the lifetime of the PCS. However, the inductors and switches in the auxiliary circuit increase the volume.

The APD for a T-type inverter is proposed[10]-[11]. This method uses only the grid-tied inductor to control the output current and the neutral point current, so no auxiliary circuit is required. Reference [10] proposes the control method using continuous current mode (CCM) in the T-type inverter to achieve APD. The APD method with CCM controls the output current and the neutral point current using a shared inductor current. Thus, the neutral point current is limited to the output current. As a result, the pulsation remains in the DC input current under CCM operation. Reference [11] proposes the control method using discontinuous current mode (DCM) in the T-type inverter to achieve APD. The APD method with DCM independently controls the output current and the neutral point current by setting a zero current period. However, the efficiency with DCM decreases due to the increase in the RMS value of the inductor current.

This paper proposes a T-type inverter that operates in both CCM and DCM control for the active power decoupling capability. The proposed method uses the DCM only during the uncontrollable periods of the CCM. Therefore, CCM/DCM control achieves APD in all periods and improves efficiency compared to DCM. However, the efficiency improvement effect is limited due to the dominant loss during the DCM period. Hence, the efficiency improvement method is applied to CCM/DCM control. The efficiency improvement method consists of two parts. In (i), the neutral point current's switching pattern is changed to reduce the RMS value of the inductor current. In (ii), determine the CCM's switching frequency that minimizes losses based on the loss analysis. A 1-kW prototype evaluates the validity of the proposed method. As a result, the proposed CCM/DCM control reduces the second harmonic components of the input current by 90.1% compared with not using the APD operation. In addition, the efficiency improvement method improves the efficiency from 90.1% to 92.5%.

II. ACTIVE POWER DECOUPLING METHOD

Figure 1 shows the configuration of a single-phase T-type inverter. The DC link capacitors C_1 and C_2 are used as energy buffers in a T-type inverter. Assuming that the power factor of

the output current is unity, the instantaneous output power p_{out} is expressed as

$$p_{out} = v_{out} i_{out} = V_{out} I_{out} - V_{out} I_{out} \cos(2\omega t) \quad (1),$$

where v_{out} is the output voltage, V_{out} is the RMS value of the output voltage, i_{out} is the output current, I_{out} is the RMS value of the output current, and ω is the grid angular frequency.

Figure 2 shows the principle of active power decoupling. The DC input power should be constant, whereas the instantaneous output power oscillates at twice the grid frequency. The power pulsation is compensated by the charge and discharge of the buffer capacitor, as shown in Fig. 2. In order to control buffer power, the two capacitor voltages v_{c1} and v_{c2} fluctuate in opposite phase. The capacitor voltages v_{c1} and v_{c2} are expressed as

$$\begin{cases} v_{c1} = \dfrac{V_{dc}}{2} - V_c \sin(\omega t + \dfrac{\pi}{4}) \\ v_{c2} = \dfrac{V_{dc}}{2} + V_c \sin(\omega t + \dfrac{\pi}{4}) \end{cases} \left(V_c \le \frac{V_{dc}}{2} \right) \quad (2),$$

where V_c is the amplitude of the capacitor voltage, and V_{dc} is the DC voltage. Note that the V_c must be lower than half of the V_{dc}. From (2), the capacitor currents i_{c1} and i_{c2} are expressed as

$$\begin{cases} i_{c1} = -\omega C_1 V_c \sin(\omega t - \dfrac{\pi}{4}) \\ i_{c2} = \omega C_2 V_c \sin(\omega t - \dfrac{\pi}{4}) \end{cases} \left(V_c \le \frac{V_{dc}}{2} \right) \quad (3),$$

where C_1 and C_2 are the capacitance of the buffer capacitor. From (1)-(3), the amplitude of the capacitor voltage V_c is determined. Then, V_c is expressed as

$$V_c = \sqrt{\frac{P_{out}}{\omega C_1}} \quad (4).$$

From (3)-(4) and Kirchhoff's law, the neutral point current i_n is expressed as (5).

$$i_n = i_{c2} - i_{c1} = 2\sqrt{\omega C_1 P_{out}} \sin(\omega t - \frac{\pi}{4}) \quad (5).$$

The T-type inverter needs to control the neutral point current so that the capacitor voltage agrees with (2). As a result, the APD is achieved without the auxiliary circuit.

III. Conventional APD Method

A. Continuous Current Mode

Figure 3 shows the absolute value of the output current command and the neutral point current command. The CCM operation controls the neutral point current with a constant current flow on the output side. A part of the output current is controlled as the neutral point current. Hence, the neutral point current does not flow more than the output current. In addition, there are periods when the neutral point current does not match the command value due to the situation of the inverter output voltage command and capacitor voltages. In this paper,

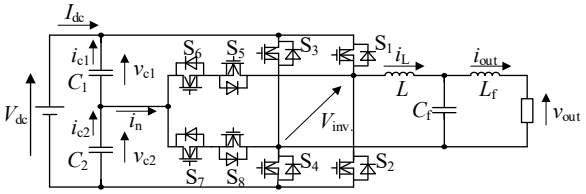

Fig. 1. Circuit configuration of a T-type inverter.

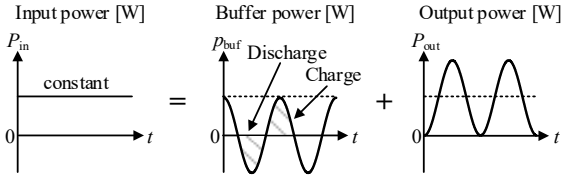

Fig. 2. Principle of active power decoupling.

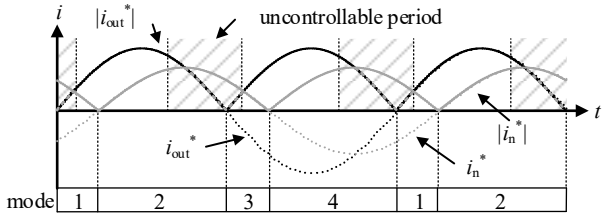

Fig. 3. Absolute value of output current command and neutral point current command.

the period when the neutral point current does not match the command value is called the uncontrollable period. If the neutral point current is controlled with priority over the output current during the non-compensated period, output current distortion occurs. Output current control is prioritized over neutral point current control during the uncontrollable period in order to prevent output current distortion.

Figure 4 shows the operating waveform for one switching cycle in the CCM operation. The T-type inverter outputs the capacitor voltage v_{cx} (v_{c1} or v_{c2}) when the inductor current i_L flows through the neutral point into the buffer capacitor. In Fig. 4, D_{out} is the period when the T-type inverter outputs the DC voltage, and D_n is the period when the T-type inverter outputs the buffer capacitor voltage. From the duty ratio command, the inverter output voltage command $v_{inv.}^*$ is expressed as (6), and the neutral point current command $|i_n^*|$ is expressed as (7).

$$v_{inv.}^* = D_{out} V_{dc} + D_n v_{cx} \quad (6),$$

$$|i_n^*| = D_n |i_{out}^*| \quad (7).$$

From (6) and (7), the duty ratio commands D_{out} and D_n are expressed as

$$D_{out} = \frac{v_{inv.}^* - D_n v_{cx}}{V_{dc}}, \quad D_n = \frac{|i_n^*|}{|i_{out}^*|} \quad (8).$$

The buffer capacitor output $D_n v_{cx}$ exceeds v_{inv}^* when the output voltage command is low, and the neutral point current command is large in (8). In this period, the output voltage does not match the inverter output voltage command $v_{inv.}^*$ because $D_{out} < 0$. The duty ratio command is limited in order to match the inverter output voltage and command value when $D_{out} < 0$. The duty ratio commands in the limited situation are expressed as

$$D_{\text{out}} = 0, \quad D_{\text{n}} = \frac{v_{\text{inv.}}}{v_{\text{cx}}} \quad (D_{\text{out}} < 0) \qquad (9).$$

On the other hand, the percentage of D_{n} in a switching cycle is significant for large $|i_{\text{n}}^*|$ situations. However, the $D_{\text{n}}v_{\text{cx}}$ is small when the buffer capacitor voltage v_{cx} is low. Over-modulation ($D_{\text{out}} + D_{\text{n}} > 1$) occurs in this case since the significant D_{out} is required. Hence, the duty ratio commands are limited to Dout + Dn = 1 when there is an over-modulation. The duty ratio commands in the over-modulation are expressed as

$$D_{\text{out}} = 1 - D_{\text{n}}, \quad D_{\text{n}} = \frac{v_{\text{inv.}} - V_{\text{dc}}}{v_{\text{cx}} - V_{\text{dc}}} \quad (D_{\text{out}} + D_{\text{n}} > 1) \quad (10).$$

Table 1 shows the switching table of the CCM operation. The CCM operation controls the neutral point current except during the uncontrollable period, according to Table 1 and (8)-(10).

Figure 5 shows the control block diagram of the CCM operation. The CCM operation usually calculates duty ratio command based on (8). The duty ratio commands are limited based on (9)-(10) when over-modulation or $D_{\text{out}} < 0$. Therefore, the neutral point current does not match the command value in the CCM operation. As a result, the pulsation remains in the DC input current under CCM operation.

B. Discontinuous Current Mode

Figure 6 shows the operation waveforms for one switching cycle in the DCM operation. The DCM operation has a zero-current period, where the inductor current becomes zero and all the switching devices are turned off. For this reason, the interference of the two current controls is solved by flowing each current during the zero-current period of the other current. There are two switching patterns in the DCM operation. The neutral point current direction in Fig. 6(a) is the opposite direction for output current i_{out}. On the other hand, the neutral point current direction in Fig. 6(b) is the same direction for output current i_{out}. The Fig. 6(b) pattern reduces the RMS value of inductor current i_{L} compared to the pattern in Fig. 6(a).

Figure 7 shows the control block diagram of the DCM operation. The duty ratios $d_1 \sim d_2$ are calculated from the inductance of the grid-tied inductor, the applied voltage, the current commands, and the switching period. The grid-tied inductor voltage fluctuates significantly during the one-switching cycle in the DCM operation. This is because two currents with different paths are controlled during the one switching cycle. Thus, discretization errors occur in both the output current i_{out} and neutral point current i_{n}. In order to reduce the discretization error, proportional control is applied for the DCM operation. Proportional control uses the low-side buffer capacitor voltage v_{c2} and the output current i_{out}. However, the peak and RMS values of the inductor current are more significant than those of the CCM operation. Therefore, the DCM operation decreases the efficiency compared to the CCM operation.

IV. PROPOSED CCM/DCM CONTROL

A. Switching the current mode

Figure 8 shows the waveforms of the current mode change in the CCM/DCM control. The proposed method switches from the CCM to the DCM in the uncontrollable periods of

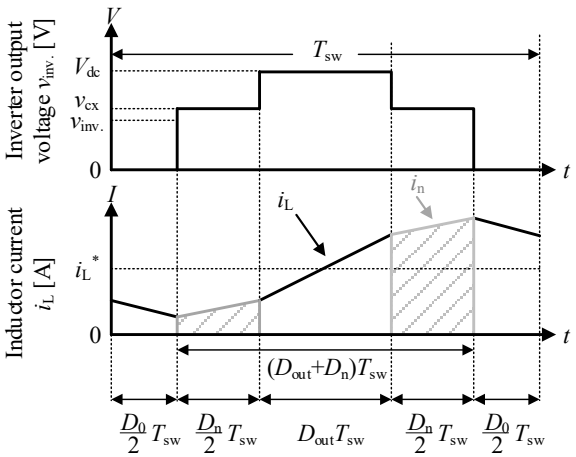

Fig. 4. Operating waveform in the CCM operation.

Table 1. Switching table of the CCM operation.

mode	control	$v_{\text{inv.}}$	S_1	S_2	S_3	S_4	S_5	S_6	S_7	S_8
1	i_{out}^*+	V_{dc}	D_{out}	off	off	ON	off	off	off	off
	i_{n}^*-	v_{c2}	off	off	off		off	D_{n}	off	off
	0 V	0	off	D_0	off		off	off	off	off
2	i_{out}^*+	V_{dc}	ON	off	off	D_{out}	off	off	off	off
	i_{n}^*+	v_{c1}		off	off	off	off	off	off	D_{n}
	0 V	0		off	D_0	off	off	off	off	off
3	i_{out}^*-	$-V_{\text{dc}}$	off	D_{out}	ON	off	off	off	off	off
	i_{n}^*+	$-v_{\text{c1}}$	off	off		off	D_{n}	off	off	off
	0 V	0	D_0	off		off	off	off	off	off
4	i_{out}^*-	$-V_{\text{dc}}$	off	ON	D_{out}	off	off	off	off	off
	i_{n}^*-	$-v_{\text{c2}}$	off		off	off	off	off	D_{n}	off
	0 V	0	off		off	D_0	off	off	off	off

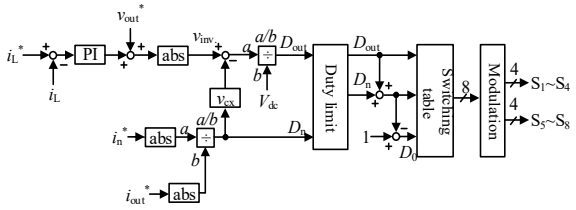

Fig. 5. Control block diagram of the CCM operation.

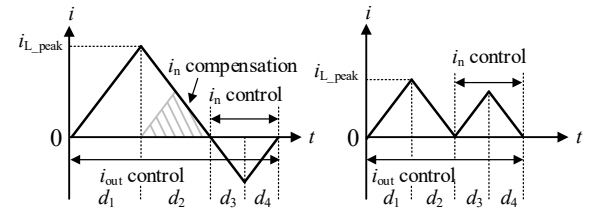

(a) i_{out} and i_{n} different polarity (b) i_{out} and i_{n} same polarity

Fig. 6. Operating waveform in the DCM operation.

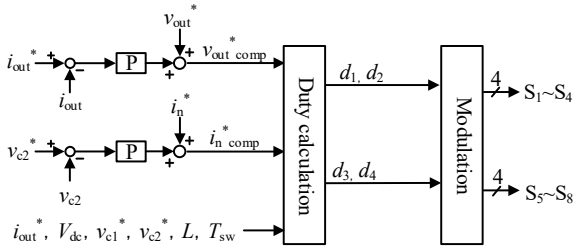

Fig. 7. Control block diagram of the DCM operation.

the CCM. As a result, the performance of the APD is improved compared to the CCM operation only. In addition, the RMS value of the inductor current is reduced compared to the DCM operation only. Consequently, the CCM/DCM control achieves APD in all periods and improves efficiency compared to DCM.

Figure 9 shows the control block diagram of the CCM/DCM control. The CCM/DCM control has separate controllers for each current mode. Each controller switches duty ratio commands based on the current mode-switching equation. The current mode-switching equation is expressed as

$$|v_{out}^{*}| - \frac{|i_n^{*}|}{|i_{out}^{*}|} V_{cx} \begin{cases} \geq 0 : \text{CCM} \\ < 0 : \text{DCM} \end{cases} \quad (11).$$

Current mode switching is performed at the time of each duty command update. In this paper, the update timing of the duty ratio command is synchronized with the bottom of the carrier. The error in switching timing to the DCM becomes significant when the carrier frequency of the CCM is low since the period of command value update depends on the carrier frequency. In order to reduce the error in switching timing, the carrier frequency of the CCM is set higher than the carrier frequency of the DCM.

Each current mode's operation ratio and loss characteristics affect efficiency in the CCM/DCM control. The CCM is dominated by switching losses in the turn-on and turn-off of switching devices. On the other hand, the DCM is dominated by conduction losses due to the high peak and RMS value of the inductor current. Therefore, the efficiency improvement method is applied to CCM/DCM control.

B. Efficiency improvement in CCM

Grid-tied inductors are generally designed with a percent impedance $\%Z_L$ of about 5% in the CCM operation. However, the CCM/DCM control requires using inductors with a lower percent impedance than typical grid-tied inductors. This is because the DCM operation requires a low percentage impedance of the grid-tied inductor. The switching ripple becomes large when the %ZL of the grid-tied inductor and the switching frequency during the CCM operation is low. As a result, there is a period when the inductor current flows in the opposite direction to the output current command. In order to prevent current flow in the opposite direction to the command value, the switching frequency during the CCM operation is set to 50 kHz in CCM/DCM control. The conventional CCM/DCM control causes high switching losses P_{sw} due to the 50 kHz switching frequency of the CCM operation. On the other hand, the switching losses P_{sw} decrease when the switching frequency of the CCM operation is reduced. However, the conduction losses P_{cond} increase because the inductor current flows in the opposite direction to the command value.

Therefore, there is a trade-off between P_{sw} and P_{cond} for the losses in the CCM operation. This trade-off depends on the switching frequency in the CCM operation. This paper determines the switching frequency that minimizes the sum of P_{sw} and P_{cond} based on the loss analysis. Improve the efficiency of the CCM operation in the CCM/DCM control by selecting the switching frequency with the lowest loss.

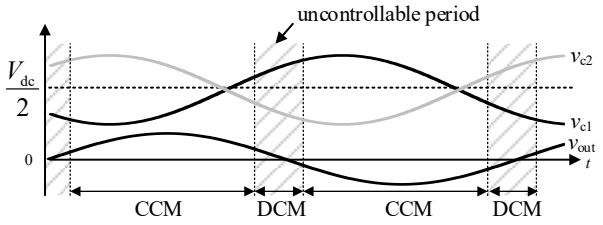

Fig. 8. Waveforms of current mode changing in the CCM/DCM control.

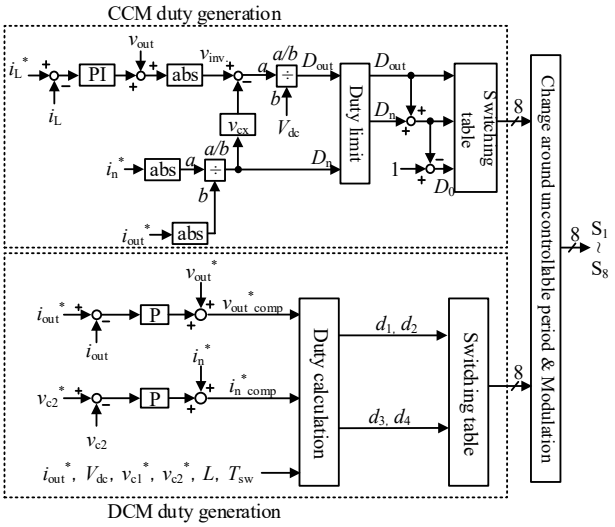

Fig. 9. Control block diagram of the CCM/DCM control.

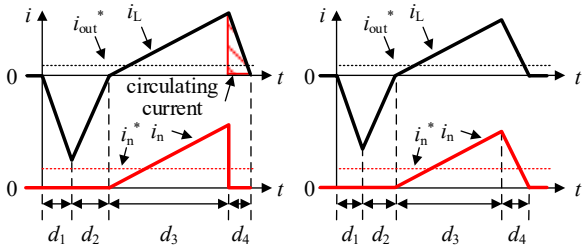

(a) Conventional control (b) Proposed control

Fig. 10. Neutral point current in the DCM operation.

C. Efficiency improvement in DCM

Figure 10 shows the conventional and proposed waveforms for the neutral point current under the DCM operation. This figure focuses on the period when the output current command i_{out}^{*} and neutral point current command i_n^{*} are positive. Furthermore, Fig. 10 shows the period when the output current command i_{out}^{*} is larger than the neutral point current command i_n^{*}. The current controller adjusts the inductor current in the d_1 and d_2 periods when the output current flows to the grid-tied inductor more than the command value by the neutral point current control. As a result, the average value of the inductor current matches the output current command value. The conventional method controls the neutral point current in the sawtooth pattern in Fig. 10(a). In this method, the circulating current flows from the grid-tied inductor during the d_4 period. The circulating current increases during the d_4 period around the peak of the neutral point current command i_n^{*}. Thus, the RMS value of the inductor current also increases during the d_1 and d_2 periods.

The proposed method controls the neutral point current in the triangular pattern in Fig. 10(b). In this method, the circulating current does not flow from the grid-tied inductor

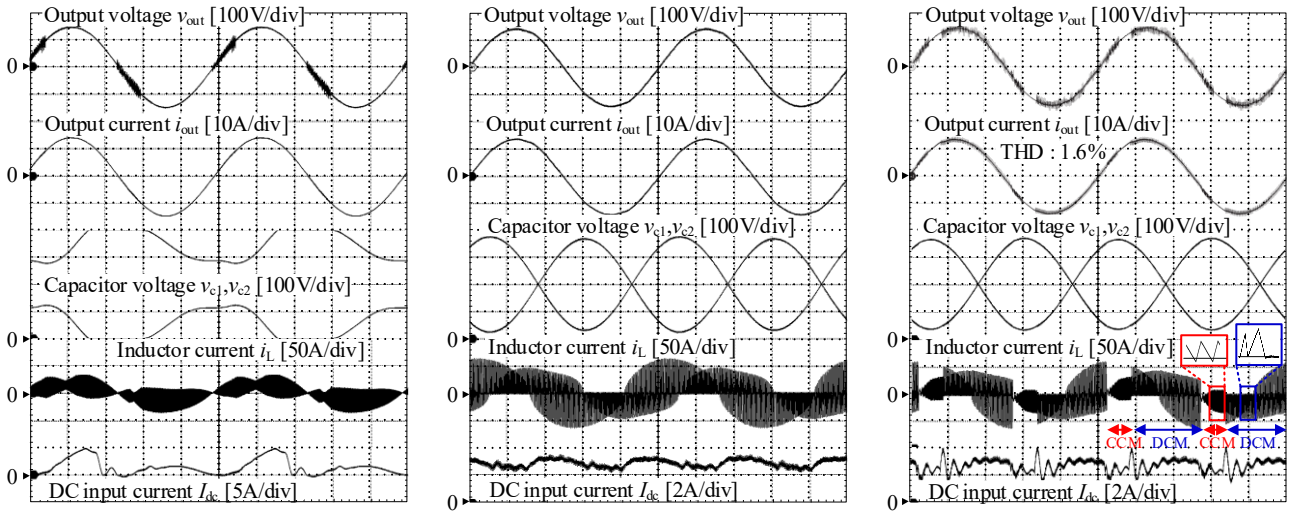

(a) CCM (b) DCM (c) Proposed

Fig. 11. Experimental results at 1 kW in each current mode.

during the d_4 period. Thus, the triangular pattern reduces the inductor current flowing during the d_1 and d_2 periods. In addition, the triangular pattern reduces the RMS value of the neutral point current compared to the sawtooth pattern. As a result, the efficiency of the DCM operation in the CCM/DCM control is improved.

V. Experimental Result

In order to verify the validity, a 1-kW prototype tests the proposed method. Table 2 shows the experimental conditions. From (4), design the capacitance of the buffer capacitor. In this paper, the buffer capacitor is 120 µF, so the amplitude of the capacitor voltage V_c is 80% of $V_{dc}/2$.

Figure 11 shows the experimental results for each current mode. The v_{c1} and v_{c2} are unbalanced due to the uncontrollable period with CCM operation in Fig. 11(a). Thus, the pulsation remains in the DC input current under the CCM operation. From Fig. 11(b), the capacitor voltages v_{c1} and v_{c2} fluctuate in opposite phases by controlling the neutral point current. As a result, the DCM operation compensates for pulsation in the DC input current, although the inductor current is increased. The inductor current in the CCM/DCM control contains the CCM operation and the DCM operation. As a result, the CCM/DCM control simultaneously compensates the pulsation components of the DC input current with a low inductor current in Fig. 11(c). Switching between the CCM operation and the DCM operation is performed without current distortion, so the output current THD in the CCM/DCM control is 1.6%.

Figure 12 shows the loss analysis result in the CCM operation period. The circuit simulator PLECS is used for the analysis. For this analysis, the thermal model is created from the datasheet of the switching device (SCT3022KL) to calculate the conduction losses and the switching losses. The analysis changes the switching frequency from 10 kHz to 50 kHz. The sum of the conduction losses and the switching losses is minimized at the switching frequency of 20 kHz in Fig.12. Thus, the switching frequency is set to 20 kHz during the CCM operation in the CCM/DCM control.

Figure 13 shows the DC input current harmonic analysis results for each current mode. The CCM operation reduces the second harmonic components by 68.5% because of the

Table 2. Experimental condition.

Parameter	Symbol	Value
Output power	P_{out}	1 kW
Input voltage	V_{dc}	400 V
Output voltage	V_{out}	100 V
Output frequency	f_{out}	50 Hz
Compensated capacitor	C_1,C_2	120 µF
Grid-tied inductor	L_1	95 µH(%Z 0.3%)

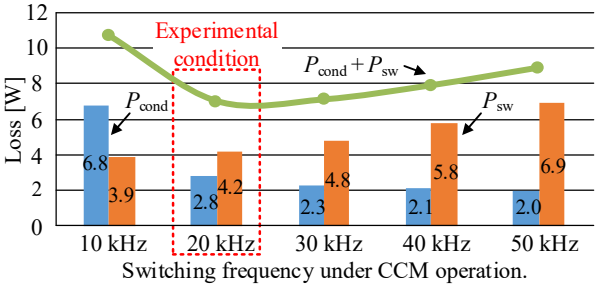

Fig. 12. Loss analysis results in the CCM operation period.

uncontrollable periods for neutral point current. In contrast, the second harmonic components are reduced by nearly 90% in the CCM/DCM control and the DCM operation because the neutral point current agrees with the command value for the APD operation in all periods.

Figure 14 shows the efficiency characteristics with only CCM operation and only DCM operation. The DCM operation with the efficiency improvement method improves the efficiency from 89.0% to 91.3% at 1 kW compared to the conventional DCM operation. In this case, the proposed DCM operation reduces the loss by 22.9% compared to the conventional DCM operation. On the other hand, the CCM operation with the efficiency improvement method improves the efficiency from 95.7% to 96.3% at 1 kW compared to the conventional CCM operation. In addition, the proposed CCM operation reduces the loss by 14.5% compared to the conventional CCM operation.

Figure 15 shows the efficiency characteristics with conventional and proposed CCM/DCM control. The proposed CCM/DCM control improves the efficiency from 90.1% to

92.5% at 1 kW compared to the conventional CCM/DCM control. In addition, the proposed CCM/DCM control reduces the loss by 14.5% compared to the conventional CCM/DCM control. Fig. 14 and Fig. 15 indicate that efficiency improvement methods contribute more to the efficiency improvement of CCM/DCM control in the DCM operation than in the CCM operation. However, the efficiency of the proposed CCM/DCM control is similar to the efficiency of the DCM operation. This is because the DCM operation accounts for 74% of one cycle under the experimental conditions of this paper.

Figure 16 shows the loss analysis results with conventional and proposed CCM/DCM control. The proposed CCM/DCM control reduces the conduction loss of the body diode in the inverter-side switch by 53.5%. This is because the efficiency improvement method of the DCM operation reduces the circulating current.

VI. Conclusion

This paper proposed the active power decoupling method based on the CCM/DCM operation for a T-type inverter. The CCM/DCM control uses the DCM only during the uncontrollable periods of the CCM to achieve active power decoupling in all periods and improve efficiency compared to DCM. As the experimental result, the THD of the output current was 1.6% in the CCM/DCM control. In addition, the second harmonic component of the DC input current was reduced by 94.2%. Furthermore, the efficiency improvement method improved the efficiency from 90.1% to 92.5% and reduced losses by 26.2%. The range of CCM operations needs to be extended for further efficiency improvement. In future work, the control method to expand the operating range of the CCM operation will be considered.

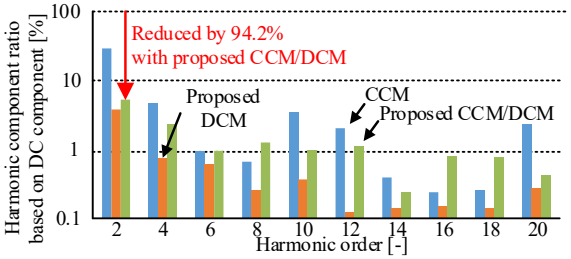

Fig. 13. Harmonic components of input current in each current mode.

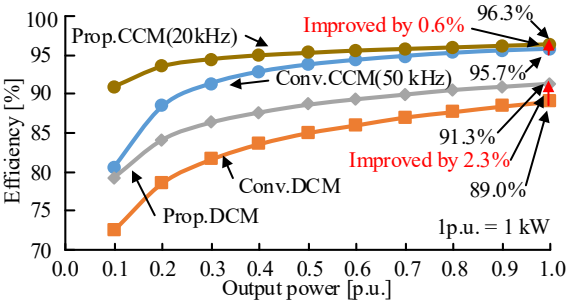

Fig. 14. Efficiency characteristics with only CCM operation and only DCM operation.

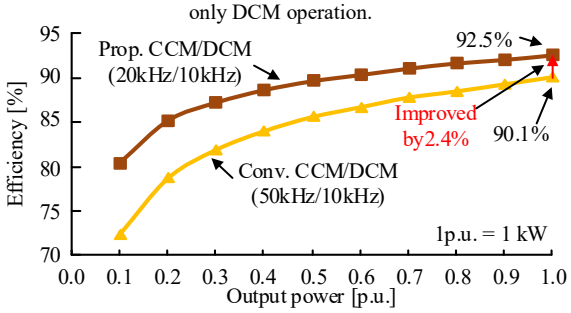

Fig. 15. Efficiency characteristics with conventional and proposed CCM/DCM control.

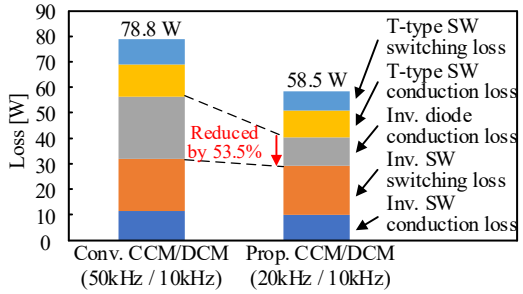

Fig. 16. Loss analysis results with conventional and proposed CCM/DCM control.

References

[1] V. Seshagiri Rao and K. Sundaramoorthy, "Performance analysis of voltage multiplier coupled cascaded boost converter with solar PV integration for DC microgrid application," IEEE Trans. on Industry Applications, vol. 59, no. 1, pp. 1013-1023, 2023

[2] D. Neumayr, G. C. Knabben, E. Varescon, D. Bortis and J. W. Kolar "Comparative evaluation of a full-and partial-power processing active power buffer for ultracompact single-phase DC/AC converter ststems," IEEE Journal of Emerging and Selected Topics in Power Electronics, vol. 9, no.2, pp. 1994-2013, 2021

[3] Y. Shen, D. Zakzewski, A. Hasnain, R. Resalayyan and A. Khaligh, "Reduced sensor control approach for active power decoupling circuit in PV microinverter application," 2023 IEEE Energy Conversion Congress and Exposition, pp. 13-18 2023

[4] T. Wei, A. Cervone and D. Dujic, "Second harmonic ripple voltage suppression for single-phase ISOP Solid-State Transformer by active power decoupling," IEEE Applied Power Electronics Conference and Exposition, pp. 1496-1502, 2023

[5] S. Qin, Y. Lei, C. Barth, W. Liu and R. C. N. Pilawa-Podgurski, "A high-efficiency high energy density buffer architecture for power pulsation decoupling in grid-interfaced converters," IEEE Energy Conversion Congress and Exposition, pp. 149-157, 2015

[6] N. Takaoka, H. Watanabe and J. Itoh, "Isolated DC to Single-Phase AC Converter with Active Power Decoupling Capability Using Coupled Inductor," IEEJ Jounal of Industry Applications, vol. 11, no. 2 pp. 341-350, 2022

[7] X. Xu, M. Su, Y. Sun, B. Guo, H. Wang and G. Xu, "Four-switch single-phase common-ground PV inverter with active power decoupling," IEEE Trans. on Industrial Electronics, vol. 69, no. 3 pp. 3223-3228, 2022

[8] T. Sekiguchi and K. Wada, "Active power decoupling Control for Single-phase Power Conditioning Systems Focusing on Harmonic Voltage," IEEJ Jounal of Industry Applications, vol. 12, no. 4 pp. 808-815, 2023

[9] S. Komeda, S. Takuma, Y. Ohnuma, R. Gondo, D. Maezaki and N. Taguchi, "Operation Characteristics of Discontinuous Current Mode for a Dual-Active-Bridge AC-DC Converter with an Active Energy Buffer," IEEJ Jounal of Industry Applications, vol. 12, no. 5 pp. 1015-1024, 2023

[10] M. Abe, H. Haga and S. Kondo, "Power decoupling method NPC single-phase AC/DC converter using neutral point voltage control," IEEJ Trans. on Industry Applications, vol. 136-D, no. 12 pp. 937-943, 2016

[11] A. Omomo, N. Takaoka, H. N. Le, K. Kusaka and J. Itoh, "T-type NPC inverter with active power decoupling capability using discontinuous current mode," European Conf. on Power Electronics and Applications, pp. 1-10, 2018